



# *Chapter 2*



Materials and methods

## 2.1 Chemicals and reagents

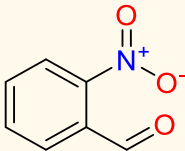
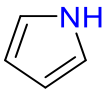
Creatinine (98 %) was procured from Alfa Aesar; potassium chloride (KCl), copper sulphate pentahydrate ( $\text{CuSO}_4 \cdot 5\text{H}_2\text{O}$ ), acetonitrile (ACN), glucose, sodium hydroxide (NaOH) pellets, sulphuric acid ( $\text{H}_2\text{SO}_4$ ) and ethanol (EtOH) from Merck; cobalt chloride hexahydrate ( $\text{CoCl}_2 \cdot 6\text{H}_2\text{O}$ ), cuprous iodide (CuI), albumin, pyrrole, uric acid, ascorbic acid and dopamine from Sigma-Aldrich; 2-nitrobenzaldehyde, urea and dipotassium hydrogen phosphate ( $\text{K}_2\text{HPO}_4$ ) from SRL; potassium dihydrogen phosphate ( $\text{KH}_2\text{PO}_4$ ) and potassium nitrate ( $\text{KNO}_3$ ) from Rankem. All these chemicals were of analytical grade and were used without further purification.

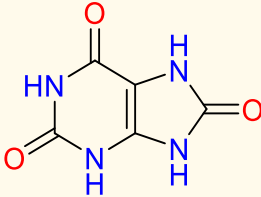
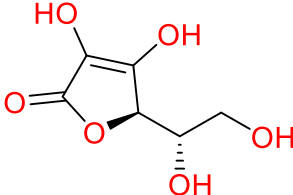
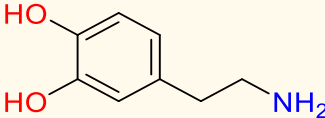
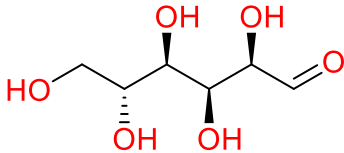
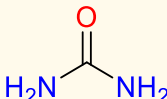
Phosphate buffer saline (PBS) solutions of 0.1 M strength, having different pH, were prepared by mixing  $\text{K}_2\text{HPO}_4$  and  $\text{KH}_2\text{PO}_4$  in an aqueous 0.1 M KCl solution. The Henderson–Hasselbalch equation was used to calculate the required amounts of  $\text{K}_2\text{HPO}_4$  and  $\text{KH}_2\text{PO}_4$  for different pH.

## 2.2 Chemical structures

Apart from the chemical structure of creatinine that is discussed in Chapter 1, the chemical structure of some other key compounds used in this thesis work, are presented in Table 2.1.

Table 2.1: Chemical structure of some compounds.

Name	Chemical Structure
2-nitrobenzaldehyde	
Pyrrole	

Uric acid	
Ascorbic acid	
Dopamine	
D-glucose	
Urea	

## 2.3 Instruments

Electrochemical analyses were carried out with Biologic SP-300 (EC-Lab software setup); JSM 6390LV (JEOL, Japan) was used to obtain the Scanning Electron Microscope (SEM) images; Powder X-Ray Diffraction (P-XRD) patterns were obtained with Bruker D8 ADVANCE ECO P-XRD; Fourier Transform Infrared Spectroscopy (FTIR) spectra were recorded with PerkinElmer, L1600300 Spectrum TWO LiTa, 91,267, (Llantrisant, UK); RENISHAW basis series with 514 lasers (RENISHAW, UK) was used to record the Raman spectra; Ultraviolet-visible (UV-vis) spectra and Diffuse Reflectance Spectra (DRS) were recorded with UV-2600I (Shimadzu); Energy dispersive X-Ray (EDX)

spectra were recorded with EDX: Model No: 7582 (Oxford make); JES-FA200 (JEOL) was used to record the Electron Paramagnetic Resonance (EPR); Conductivity measurements were carried out with Systronics conductivity meter (Type: 304, Sr. No. 13,408); lattice parameters were recorded with Bruker AXS SMART APEX-II Single crystal X-ray diffractometer (software: APEX-II).

## 2.4 Electrode cleaning, maintenance and connections

All the electrochemical analyses were carried out with the 3-electrodes set-up: working electrode (WE), reference electrode (RE) and counter electrode (CE). While a glassy carbon electrode (GCE) with 3 mm diameter or a platinum (Pt) electrode (polycrystalline, 99.99%) with 2 mm diameter was used as the WE, an Ag/AgCl/KCl (3.5 M) electrode was used as the RE and a Pt-wire as the CE. Proper cleaning and maintenance of these electrodes greatly ensure the accuracy of the electrochemical responses. Thus, these are some necessary steps in electrochemical analysis.

The most frequently performed process to ensure the cleanliness of the WE was to polish its surface with a slurry of alumina powder (of sizes 1 micron, 0.3 micron and 0.05 micron), on polishing pads made of nylon or cloth. The WE polishing step was implemented before every new run. At times, the surface of the WE was also sonicated in ethanol or distilled water, and multiple cyclic voltammetry (CV) runs in dilute H<sub>2</sub>SO<sub>4</sub> with the bare WE were also done to remove any surface contamination. The WE was always cleaned, dried and stored in a sealed pack when not in use.

On the other hand, the RE was always stored by dipping in an electrolyte solution (diluted KCl) when not in use to keep the frit wet for proper operation. The frit allows the movement of ions through it. Hence, changing the electrolyte solution inside the RE was also frequently practised to ensure that the electrolyte solution stayed non-contaminated with intact concentration.

The CE was wiped properly with wet tissues and dried, before every new run. At times, it was also sonicated in distilled water for cleaning. Similar to the storage conditions of WE, the CE was also always cleaned, dried and stored in a sealed pack when not in use.

The electrodes are connected to the electrochemical workstation via alligator clips. After every few runs, the contact points in the alligator clips are gently wiped with tissue and emery paper to remove any dirt or moisture adsorbed from the environment.

## 2.5 Methods

### 2.5.1 Electrochemical methods

Several electrochemical methods like cyclic voltammetry (CV), differential pulse voltammetry (DPV), chronoamperometry (CA), chronopotentiometry (CP) and electrochemical impedance spectroscopy (EIS) have been used in this thesis work for determining redox potentials and peak currents of known and newly synthesized compounds, analyzing solutions and solution mixtures from electrochemical point of view, modifying electrode surface, establishing reaction mechanisms, optimizing reaction conditions, as transduction systems for the developed creatinine sensors, etc. The fundamentals of each of these electrochemical methods have been provided below.

#### 2.5.1.1 Cyclic Voltammetry

CV is perhaps the most commonly employed and the foremost choice amongst the electrochemical techniques, to study the redox behaviour of electroactive species. In CV experiments, a linear sweep of potential on the WE, relative to the RE, is carried out and the current response is recorded. The potential is firstly swept linearly from an initial potential ( $E_1$ ) to a switching potential ( $E_2$ ), which is called the forward scan. Once  $E_2$  is reached, the potential is swept in the opposite direction, back to  $E_1$ , which is called the reverse scan. The forward and the reverse scan constitute one complete cycle, as the potential reaches its initial value, and by repeating the process, multiple cycles can be run. Figure 2.1 (A) shows a plot of the potential sweep (V) against time (s) during a typical CV experiment. As seen in the figure,  $T_2$  is the time required to complete one cycle and  $T_4$  is the time required to complete two cycles.

The current or current density at the WE is recorded as the response signal during the potential scans. A duck-shaped graph is obtained by plotting the current response against the potential as in a typical cyclic voltammogram. Figure 2.1 (B) represents a simple cyclic voltammogram with one redox couple for an electroactive species, say M. According to the IUPAC convention,  $E_2 > E_1$ , and anodic peaks are obtained when the WE

is sufficiently oxidant during the forward scan [1]. An anodic peak is shown at the potential  $E_{pa}$  for the oxidation of  $M$  to  $M^{n+}$  (where 'n' is the number of transferred electrons) in Figure 2.1 (B). During the reverse scan, cathodic peaks are obtained when the working electrode is sufficiently reductant [1]. A cathodic peak is shown at the potential  $E_{pc}$  for the reduction of  $M^{n+}$  to  $M$  in Figure 2.1 (B). According to the US convention,  $E_2 < E_1$ , and accordingly, the redox processes interchanges for each scan direction [1]. The intensity of the anodic peak current ( $i_{pa}$ ) and the cathodic peak current ( $i_{pc}$ ), which vary with the analyte concentration, must be measured from the tip of the peaks to the extended baselines. Notably, the potential at which the curve starts shifting from the baseline due to the initiation of the redox process is called the onset potential ( $E_{onset}$ ). While the Faradaic processes (redox reactions) occur due to charge transfer across the electrode-electrolyte phase boundary, non-Faradaic or capacitive currents are also observed in the cyclic voltammograms due to the mere charging or discharging of the electrochemical double layer [2]. Only the non-Faradaic current response, without any  $E_{onset}$ , would be observed in the voltammogram of an electrochemically inactive species.

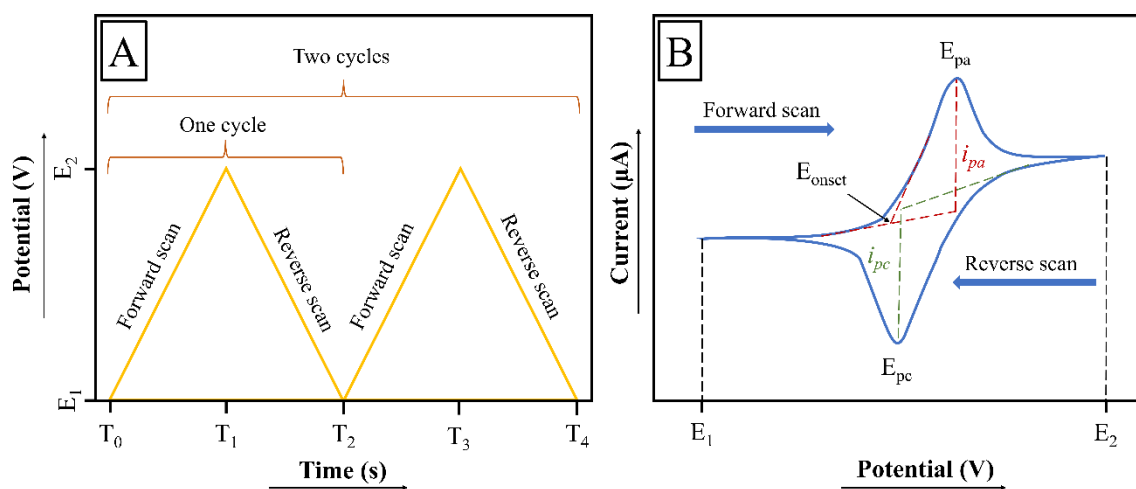


Figure 2.1: A) A potential-time waveform obtained during the CV run, and B) a typical cyclic voltammogram with one redox couple.

*Kissinger and Heinemen* [3] explained how the Nernst equation governs the rapid change in the voltammogram curves due to the redox processes. For the  $M/M^{n+}$  redox processes, the Nernst equation at 25 °C is shown in Equation 2.1, where ' $E$ ' is the potential on the WE and ' $E^\circ$ ' is the standard reduction potential for the redox couple.

$$E = E^{\circ} - \frac{0.05916}{n} \log_{10} \left( \frac{[M^{n+}]}{[M]} \right)$$

(Eq. 2.1)

At the initiation of the reverse scan,  $E > E^{\circ}$  and  $[M^{n+}] > [M]$  to satisfy the Nernst equation. As we sweep  $E$  towards lower potential, to proceed with the reverse scan, the ratio of  $[M^{n+}]$  to  $[M]$  on the electrode surface changes due to the reduction of  $[M^{n+}]$ , meanwhile, generating negligible current. A rapid change in the voltammogram curve occurs when  $E$  equals  $E^{\circ}$ , reflecting the ratio of  $[M^{n+}]$  to  $[M]$  to be 1, causing a sudden rise in the cathodic current.

An important CV parameter is ‘scan rate’, which can be defined as the rate of change in the sweeping potential per unit of time. It is comprehensible that low currents are observed with slow scan rates due to the increase in the size of the diffusion layer and high currents are observed with fast scan rates due to the decrease in the size of the diffusion layer [4]. With low scan rates, the capacitive current might also mask the Faradaic current and valuable information might be lost [5]. However, fast scan rates also have certain demerits, such as changing the electrode surface kinetics by increasing the mobility of the fresh incoming ions while quickly removing the products and causing saturation of the analog-to-digital converter due to high Faradaic current [6, 7]. Thus, at high scan rates, the reaction rate is limited by the speed of the electron transfer or kinetic processes. As the potential changes rapidly, insufficient time is left for the electrochemical reaction to occur and the kinetic information is masked, making it challenging to determine the reversibility of the system or the accuracy of analytical methods. Hence, an appropriate scan rate is required to provide enough time for certain desired reactions to occur, or it may also be used as a limiting factor to ensure that any undesired reaction doesn’t initiate. For example, *Zhu et al.* found an undesired irreversible sulfation reaction occurring at low scan rates and the scan rate of  $5 \text{ mV s}^{-1}$  was experimentally determined to ensure less sulfation reaction [8].

Scan rates are also important for studying the kinetics of the reactions. For diffusion-controlled processes, the peak current varies linearly with the square root of the scan rates (in  $\text{V s}^{-1}$ ), and for surface-controlled (adsorption-controlled) processes the peak current varies linearly with the square root. The effect of scan rate on the peak current for

reversible and diffusion-controlled processes can be mathematically described by the *Randles–Ševčík* equation. The *Randles–Ševčík* equation for reversible system is represented by Equation 2.2a where  $i_p$  is the peak current (A),  $n$  is the number of electrons transferred,  $A$  is the surface area of the WE (cm<sup>2</sup>),  $F$  is the Faraday's Constant (96,485 C/mol),  $D$  is the diffusion coefficient (cm<sup>2</sup> s<sup>-1</sup>),  $C$  is the concentration of the analyte or electroactive species (mol/cm<sup>3</sup>),  $v$  is the scan rate (V s<sup>-1</sup>),  $R$  is the gas constant (8.3144 J K<sup>-1</sup> mol<sup>-1</sup>) and  $T$  is the temperature (K).

$$i_p = 0.4463 n F A C \left( \frac{n F v D}{R T} \right)^{\frac{1}{2}} \quad (\text{Eq. 2.2a})$$

At 25 °C, the above equation takes the form:

$$i_p = 2.69 \times 10^5 n^{\frac{3}{2}} A C D^{\frac{1}{2}} v^{\frac{1}{2}} \quad (\text{Eq. 2.2b})$$

For irreversible and quasi-reversible systems, the peak current can be described by Equation 2.2c and 2.2d respectively, where  $\alpha$  is the transfer coefficient and  $K(\Lambda, \alpha)$  modified dimensionless parameter [9].

$$i_p = 2.99 \times 10^5 \alpha n (n')^{\frac{1}{2}} A C^{\frac{1}{2}} D^{\frac{1}{2}} v^{\frac{1}{2}} \quad (\text{Eq. 2.2c})$$

$$i_p = \left( 2.69 \times 10^5 n^{\frac{3}{2}} A C D^{\frac{1}{2}} v^{\frac{1}{2}} \right) K(\Lambda, \alpha) \quad (\text{Eq. 2.2d})$$

### 2.5.1.2 Differential Pulse Voltammetry

DPV is a widely used electrochemical technique, which has been designed to minimize the capacitive current and offer higher sensitivity. In a DPV experiment, the potential of the WE, relative to the RE, is ramped from an initial potential ( $E_1$ ) to a final potential ( $E_2$ ) in a series of small voltage pulses. Figure 2.2 (A) shows the potential (V) v/s time (s) waveform during a DPV run. Initially, the system is stabilized by holding it at  $E_1$ , where no redox process occurs, for a few seconds. Then the current response ( $i_l$ ) on



the WE is sampled, just before applying the first voltage pulse,  $P_1$  (in mV), as can be seen in Figure 2.2 (A). After the first pulse, the system is maintained at the constant potential for a small time interval,  $t^\circ$  (in ms). Then the current response ( $i_2$ ) is again sampled just before applying the second voltage pulse,  $P_2$ , in the reverse direction. There would be a nett increment in the potential of the WE after applying both pulses because the magnitude of  $P_2$  is smaller than  $P_1$ . The process is repeated until the potential,  $E_2$ , is reached.

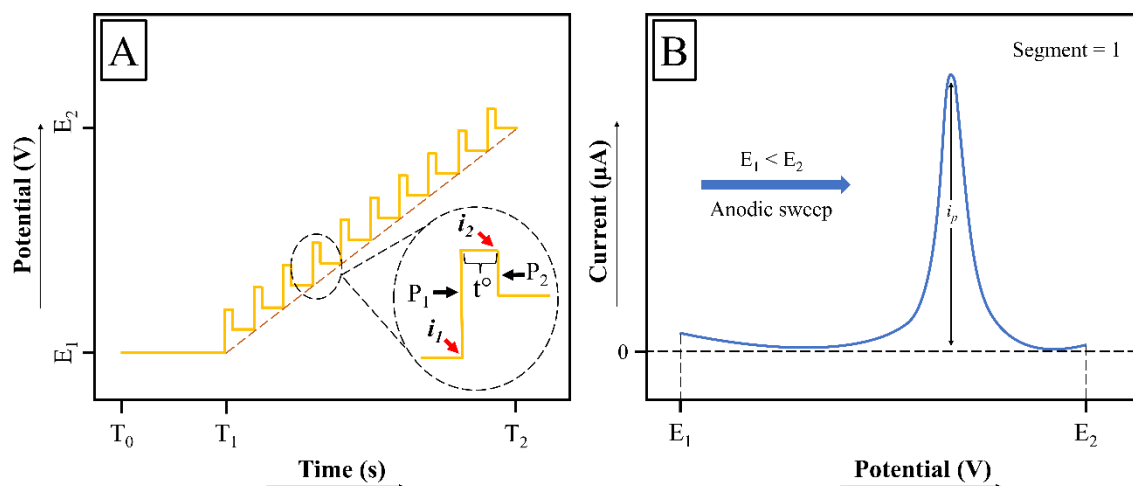


Figure 2.2: A) A potential-time waveform obtained during the DPV run, and B) a typical differential pulse voltammogram.

The current sampling process effectively minimizes the capacitive current and [10]. Hence, DPV offers higher sensitivity by generating peaks for lower concentrations of analytes and also provides better discrimination (well-separated peaks) of analytes, than the corresponding CV [11]. The voltammogram peaks are also sharper, more intense, and vary with analyte concentration. However, a demerit of this technique is the longer operation time.

The difference between the sampled currents, after and before each pulse, is plotted against the potential steps in a typical differential pulse voltammogram, as shown in Figure 2.2 (B). Figure 2.2 (B) also represents the anodic sweep of a DPV curve with only one segment. In a single segment, if the pulse sequences are moved from low potential to high potential, it is called an anodic sweep and if those are moved from high to low potential, it is called a cathodic sweep. However, commands are available in the electrochemical workstations to apply multiple segments to a DPV operation, where the system can be ramped back and forth several times between the two potentials,  $E_2$  and  $E_1$ , or even

between other potential boundaries. The application of DPV with multiple segments is rarely found in the literature.

### 2.5.1.3 Chronoamperometry

CA is a sensitive electrochemical technique which monitors current with time. In a CA experiment, the potential of the WE, relative to the RE, is initially maintained at a resting potential,  $E_0$ , where no redox reaction occurs. After that, the potential is stepped to  $E_1$ , at which oxidation or reduction of the electroactive species occurs. While CA with one potential step is mostly employed, multiple potential steps can be added. If the potential is stepped back to  $E_0$  from  $E_1$ , that will lead to the reversal of the redox reaction. The plot of potential (V) v/s time (s) during a CA run with two potential steps, is shown in Figure 2.3 (A).

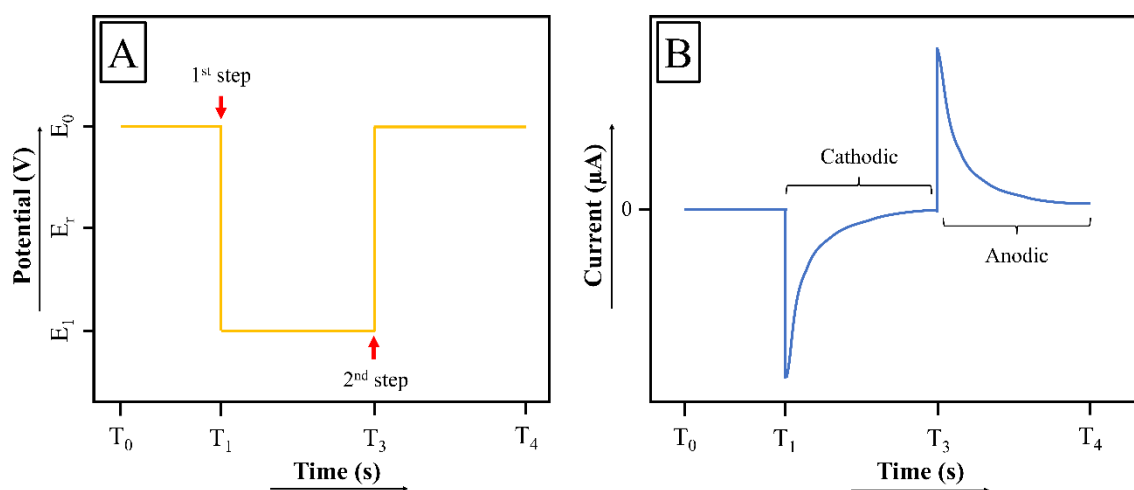


Figure 2.3: A) A potential-time waveform obtained during the CA run, and B) a typical CA graph.

Prior CV or DPV runs of the electroactive species are required to learn the potential ranges for the Faradaic and non-Faradaic processes. For a redox couple,  $M/M^{n+}$ , with a reduction potential at  $E_r$ , if the analyte is initially present at its oxidized form  $M^{n+}$  in the solution, then  $E_0$  is chosen at a higher potential than  $E_r$ ; and  $E_1$ , at a lower potential than  $E_r$ . On applying the stepped potential,  $M^{n+}$  diffuses from the bulk towards the electrode surface where it reduces to  $M$ . The Faradaic current, thus produced, decays with time as the transport limit of  $M^{n+}$  from the bulk to the electrode surface is reached. Simultaneously, the capacitive current is also generated due to the ion flux, on applying the stepped

potential. These currents exhibit an exponential decay with time [12]. As the capacitive current decays rapidly, the later part of the exponentially declining graph can be solely attributed to the decay of the Faradaic current which follows the Cottrell equation [13, 14]. Usually, the decay of the Faradaic current is noted in the last 90% of the step time. Figure 2.3 (B) represents a typical CA graph which shows a current ( $\mu\text{A}$ ) v/s time (s) response, where the first potential step led to the reduction of the analyte and the second potential step led to its oxidation.

The Cottrell equation was derived by *F. G. Cottrell* [15], which can mathematically relate the change in electric current with time, at a constant potential, for a diffusion-controlled redox process. Equation 2.3 represents the Cottrell equation where  $i_t$  is the current (A) at any given time,  $n$  is the number of electrons exchanged during the redox process for one molecule,  $F$  is the Faraday's constant (96,485 C/mol),  $A$  is the surface area of WE ( $\text{cm}^2$ ),  $C_0$  is the initial concentration of electroactive species ( $\text{mol}/\text{cm}^3$ ),  $D_0$  is diffusion constant for electroactive species ( $\text{cm}^2/\text{s}$ ) and  $t$  is time (s).

$$i_t = \frac{nFAC_0D_0^{1/2}}{\pi^{1/2} t^{1/2}}$$

(Eq. 2.3)

CA offers quicker analysis than the DPV technique but lacks selectivity and cannot be employed to identify analytes. However, CA can be well-utilized for electrochemical deposition of metals or alloys [16, 17]. For the electrodeposition of metals using CA, as performed in this thesis work, the potential of the WE needs to be stepped to a value at which the metal reduces on the WE surface.

#### 2.5.1.4 Chronopotentiometry

CP is a galvanostatic method, where the current at the WE is maintained at a constant level and the change in potential is recorded with time. In a CP experiment, when constant current is applied to the WE, the potential of the WE changes to commence a flux of electroactive species towards the WE to supply the current. For example, if a  $\text{M}/\text{M}^{n+}$  redox couple is considered, the potential changes to the value at which the reduction of M to  $\text{M}^{n+}$  occurs to supply the current. After some time, as the concentration of M becomes

0 at the WE surface, the flux of the electroactive species ceases. To maintain the current flow, the potential changes to a new value at which the solvent or any other electroactive species, if present, can undergo a redox process. The time taken for this shifting of potential to occur is called the transition time ( $\tau$ ). The plot of changing potential with time is obtained in a CP graph, which can be of different forms depending on the analyte and the solvent system. The CP method has been widely explored in the literature for polypyrrole (PPy) electrodeposition [18-21].

### 2.5.1.5 Electrochemical Impedance Spectroscopy

EIS is a powerful method that offers mechanical and kinetic data of an electrochemical system [22]. When an electrochemical system is perturbed by a sinusoidal voltage or current as an input signal with varying frequencies, an output signal in the form of a sinusoidal current or voltage, respectively, is generated [23]. The obstruction in the current flow in the system is defined as the electrochemical impedance ( $Z$ ) and it depends on various attributes, including the electrode dimension and morphology, coated materials on the WE surface, properties of the electrode-electrolyte interface, type of redox species and electrolytes, etc. EIS enables the calculation of the system's frequency-dependent  $Z$  by monitoring the input and output signals.  $Z$  is unlike the frequency-independent resistance for the ideal circuit (following Ohm's law at all current and voltage) where the alternating input and output signal stay in phase through the resistor.

Let's consider that an input alternating voltage signal is applied, which can be represented by Equation 2.4.

$$E(t) = E_0 \sin(\omega t) \quad (\text{Eq. 2.4})$$

In this case, an output alternating current signal will be generated, which can be represented by Equation 2.5.

$$I(t) = I_0 \sin(\omega t - \varphi) \quad (\text{Eq. 2.5})$$

Thus,  $Z$  of the system can be derived as shown below.

$$Z = \frac{E(t)}{I(t)} = \frac{E_0 \sin(\omega t)}{I_0 \sin(\omega t - \varphi)} = |Z| \frac{\sin(\omega t)}{\sin(\omega t - \varphi)}$$

(Eq. 2.6)

Equation 2.7 represents the Euler's relationship.

$$\exp(j\varphi) = \cos\varphi + j\sin\varphi$$

(Eq. 2.7)

Using Euler's relationship,  $Z$  can also be expressed as a complex number, having a real and an imaginary part, as shown below.

$$Z = \frac{E(t)}{I(t)} = \frac{E_0 \exp(j\omega t)}{I_0 \exp(j\omega t - j\varphi)} = |Z| \exp(j\varphi) = |Z| (\cos\varphi + j\sin\varphi)$$

(Eq. 2.8)

In the above equations, ' $E(t)$ ' represents the potential at any time, ' $E_0$ ' is the amplitude of the sinusoidal voltage signal, ' $\omega$ ' is the radial frequency ( $\omega = 2\pi f$ , where  $f$  is the frequency in hertz), ' $t$ ' is the time, ' $I(t)$ ' is the potential at any time, ' $I_0$ ' is the amplitude of the sinusoidal current signal, ' $\varphi$ ' is the phase difference between the sinusoidal signals, ' $j$ ' (equals to root over -1) is an imaginary component and ' $|Z|$ ' is the magnitude of impedance.

The 'Nyquist plot' and the 'Bode plot' are popularly used to represent the EIS data. In the Nyquist plot the negative of the imaginary part of  $Z$  ( $-Z_{IM}$ ) is plotted on the Y-axis and the real part of  $Z$  ( $Z_{REAL}$ ) is plotted on the X-axis. A vector of length  $|Z|$  represents the system's impedance in a Nyquist plot. Although the real part of  $Z$  is plotted on the X-axis, the system also moves from comparatively higher to lower frequency along the axis. However, a demerit of the Nyquist plot is that the exact frequency at any point cannot be known. This problem is addressed by the Bode plot which provides the frequency information. In the Bode plot, the logarithm of the module of impedance,  $\log(|Z|)$ , and phase shift,  $\varphi$ , are plotted on different Y-axes, while the logarithm of frequency,  $\log(f)$ , is plotted on the X-axis.

The obtained impedance graph can be fitted into an equivalent circuit model, consisting of passive circuit elements like capacitors, resistors and inductors in a parallel, series or mixed combination. The circuit model also provides information about the different individual components of the circuit elements: resistance of solution ( $R_s$ ), charge transfer resistance ( $R_{ct}$ ), Warburg resistance ( $Z_w$ ), polarization resistance ( $R_p$ ), double layer capacitance ( $C_{dl}$ ), coating capacitance ( $C_c$ ) and constant phase element (CPE) [24-26]. These circuit components can be combined in hundreds of combinations, and the fitted impedance graph is unique for each. Furthermore, each of these circuit components represents an electrical, electrochemical or physical process that occurs in the system when perturbed with a sinusoidal signal, and all these processes have different time constants [22]. Among these, the three important processes that govern most of the electrochemical system upon perturbation are: 1) the charging/discharging of the electrical double layer which gives  $C_{dl}$ , 2) the diffusion of redox species from bulk to the electrode surface which gives  $Z_w$  and 3) the Faradaic reactions of the species on the electrode surface which gives  $R_{ct}$ . A major advantage of the EIS method is its ability to differentiate all these processes [22].

Randles circuit is a common equivalent circuit that consists of  $R_s$ ,  $C_{dl}$  and  $R_{ct}$  in a mixed combination, as shown in Figure 2.4. The corresponding Nyquist and Bode plots for the circuit are shown in the figure.

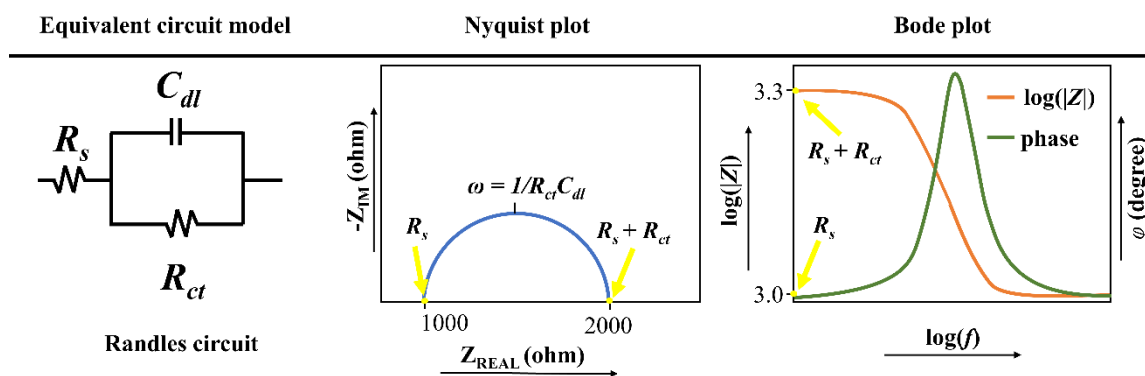


Figure 2.4: Nyquist and Bode plot for Randles circuit.

As can be seen in the Nyquist plot for the Randles circuit in Figure 2.4, a semi-circle is obtained for the resistance in the Faradaic process of the redox species. The  $R_s$  is given by the point on the X-axis at which the semi-circle intersects in the lower frequency

region. The point on the X-axis at which the semi-circle intersects in the higher frequency region gives the summation of  $R_s$  and  $R_{ct}$ . The values can also be directly read in the Bode plot, from which the time constant of the processes can also be marked.

Many equivalent circuits are experimentally obtained which are formed with added components to the Randles circuit. In those cases, the Nyquist and Bode plots accordingly change. For example, a straight line at a  $45^\circ$  angle to the X-axis is a characteristic Nyquist plot for a circuit with  $Z_w$  as a single component. When  $Z_w$  is present in a parallel combination with  $R_{ct}$ , the straight at  $45^\circ$  angle to the X-axis appears as the continuation of the semi-circle.

Nyquist plots are more frequently used in electroanalytical techniques for systems consisting of redox species. Due to the interaction of the redox species with other species in the solution or with the electrode material, the kinetics of the charge transfer reaction changes. As a result, the dimension of the semi-circle for  $R_{ct}$  also changes, which lays the foundation for EIS-based electroanalytical sensors.

### 2.5.2 Other general methods

Several other well-established methods have been used in this work, for the characterization of compounds and supporting evidence. Spectroscopic methods like FTIR and Raman have been primarily used to understand the structure and bonding of newly synthesized compounds. FTIR of liquid samples has also been recorded to analyze or predict the presence of non-isolable compounds. UV-vis spectra and DRS were recorded to analyze liquid and solid samples respectively. P-XRD was employed to establish the formation of new amorphous compounds by distinguishing the diffraction patterns of the products from the diffraction patterns of the reactants. EDX was used for elemental analysis and EPR, to establish paramagnetic properties. SEM images are also recorded for morphological characterization.

## References

- [1] Rafiee, M., Abrams, D. J., Cardinale, L., Goss, Z., Romero-Arenas, A. and Stahl, S.S. Cyclic voltammetry and chronoamperometry: mechanistic tools for organic electrosynthesis. *Chemical Society Reviews*, 53:566–585, 2024.

- 
- [2] Heinze, J. Cyclic voltammetry—"electrochemical spectroscopy". New analytical methods (25). *Angewandte Chemie International Edition in English*, 23(11):831–847, 1984.
- [3] Kissinger, P. T. and Heineman, W. R. Cyclic voltammetry. *Journal of Chemical Education*, 60(9):702, 1983.
- [4] Elgrishi, N., Rountree, K. J., McCarthy, B. D., Rountree, E. S., Eisenhart, T. T. and Dempsey, J. L. A practical beginner's guide to cyclic voltammetry. *Journal of Chemical Education*, 95(2):197–206, 2018.
- [5] Ruiz, Y., Baeza, J. A., Montpart, N., Moral-Vico, J., Baeza, M. and Guisasola, A. Repeatability of low scan rate cyclic voltammetry in bioelectrochemical systems and effects on their performance. *Journal of Chemical Technology & Biotechnology*, 95(5):1533–1541, 2020.
- [6] Aziz, S. B., Dannoun, E. M., Murad, A. R., Mahmoud, K. H., Brza, M. A., Nofal, M. M., Elsayed, K. A., Abdullah, S. N., Hadi, J. M. and Kadir, M. F. Z. Influence of scan rate on CV Pattern: Electrical and electrochemical properties of plasticized Methylcellulose: Dextran (MC: Dex) proton conducting polymer electrolytes. *Alexandria Engineering Journal*, 61(8):5919–5937, 2022.
- [7] Keithley, R. B., Takmakov, P., Bucher, E. S., Belle, A. M., Owesson-White, C. A., Park, J. and Wightman, R. M. Higher sensitivity dopamine measurements with faster-scan cyclic voltammetry. *Analytical chemistry*, 83(9):3563–3571, 2011.
- [8] Zhu, H., Li, Y., Song, Y., Zhao, G., Wu, W., Zhou, S., Wang, D. and Xiao, W. Effects of cyclic voltammetric scan rates, scan time, temperatures and carbon addition on sulphation of Pb disc electrodes in aqueous H<sub>2</sub>SO<sub>4</sub>. *Materials Technology*, 35(3):135–140, 2020.
- [9] Trachioti, M. G., Lazanas, A. C. and Prodromidis, M. I. Shedding light on the calculation of electrode electroactive area and heterogeneous electron transfer rate constants at graphite screen-printed electrodes. *Microchimica Acta*, 190:251, 2023.
- [10] Kashyap, B. and Kumar, R. A novel multi-set differential pulse voltammetry technique for improving precision in electrochemical sensing. *Biosensors and Bioelectronics*, 216:114628, 2022.
- [11] Venton, B. J. and Cao, Q. Fundamentals of fast-scan cyclic voltammetry for dopamine detection. *Analyst*, 145(4):1158–1168, 2020.
-



- 
- [12] Bard, A. J. and Faulkner, L. R. *Electrochemical Methods: Fundamentals and Applications*. John Wiley & Sons Inc., New York, USA, 2nd edition, 2000.
- [13] Kamat, A., Huth, A., Klein, O. and Scholl, S. Chronoamperometric investigations of the electrode–electrolyte interface of a commercial high temperature PEM fuel cell. *Fuel Cells*, 10(6):983–992, 2010.
- [14] Zhang, X., Philips, J., Roume, H., Guo, K., Rabaey, K. and PrévotEAU, A. Rapid and quantitative assessment of redox conduction across electroactive biofilms by using double potential step chronoamperometry. *ChemElectroChem*, 4(5):1026–1036, 2017.
- [15] Cottrell, F. G. Der Reststrom bei galvanischer Polarisation, betrachtet als ein Diffusionsproblem. *Zeitschrift für physikalische Chemie*, 42(1):385–431, 1903.
- [16] Grujicic, D. and Pesic, B. Electrodeposition of copper: the nucleation mechanisms. *Electrochimica Acta*, 47(18):2901–2912, 2002.
- [17] Zhang, J., An, M. and Chang, L. Study of the electrochemical deposition of Sn–Ag–Cu alloy by cyclic voltammetry and chronoamperometry. *Electrochimica Acta*, 54(10):2883–2889, 2009.
- [18] El Guerraf, A., Aouzal, Z., Bouabdallaoui, M., Ben Jadi, S., El Jaouhari, A., Wang, R., Bazzaoui, M. and Bazzaoui, E. A. Electrochemically roughened silver surface versus fractal leaf-shaped silver crystals for surface-enhanced Raman scattering investigation of polypyrrole. *Journal of Solid State Electrochemistry*, 23:1811–1827, 2019.
- [19] Fall, M., Diagne, A. A., Guene, M., Della Volpe, C., Bonora, P. L., Deflorian, F. and Rossi, S. R. Electrochemical properties and electrochemical impedance spectroscopy of polypyrrole-coated platinum electrodes. *Bulletin of the Chemical Society of Ethiopia*, 20(2):279–293, 2006.
- [20] Otero, T. F. and Martinez, J. G. Activation energy for polypyrrole oxidation: Film thickness influence. *Journal of Solid State Electrochemistry*, 15:1169–1178, 2011.
- [21] El Nady, J., Shokry, A., Khalil, M., Ebrahim, S., Elshaer, A. M. and Anas, M. One-step electrodeposition of a polypyrrole/NiO nanocomposite as a supercapacitor electrode. *Scientific Reports*, 12(1):3611, 2022.
- [22] Lazanas, A. C. and Prodromidis, M. I. Electrochemical impedance spectroscopy—a tutorial. *ACS Measurement Science Au*, 3(3):162–193, 2023.
-

- 
- [23] Wang, Shangshang, Jianbo Zhang, Oumaïma Gharbi, Vincent Vivier, Ming Gao, and Mark E. Orazem. Electrochemical impedance spectroscopy. *Nature Reviews Methods Primers*, 1:41, 2021.
- [24] Magar, H. S., Hassan, R. Y. and Mulchandani, A. Electrochemical impedance spectroscopy (EIS): Principles, construction, and biosensing applications. *Sensors*, 21(19):6578, 2021.
- [25] Martínez, I. and Andrade, C. Polarization resistance measurements of bars embedded in concrete with different chloride concentrations: EIS and DC comparison. *Materials and Corrosion*, 62(10):932–942, 2011.
- [26] Deflorian, F., Fedrizzi, L., Rossi, S. and Bonora, P. L. Organic coating capacitance measurement by EIS: ideal and actual trends. *Electrochimica Acta*, 44(24):4243–4249, 1999.